

Article

A Comparative Study of Cerium(III) and Cerium(IV) Phosphates for Sunscreens

Taisiya O. Kozlova ¹, Darya N. Vasilyeva ^{1,2}, Daniil A. Kozlov ¹, Irina V. Kolesnik ^{1,3},
 Maria A. Teplonogova ¹, Ilya V. Tronev ^{1,2}, Ekaterina D. Sheichenko ^{1,2}, Maria R. Protsenko ^{1,2},
 Danil D. Kolmanovich ⁴, Olga S. Ivanova ⁵, Alexander E. Baranchikov ¹ and Vladimir K. Ivanov ^{1,*}

¹ Kurnakov Institute of General and Inorganic Chemistry of the Russian Academy of Sciences, Moscow 119991, Russia

² Faculty of Chemistry, National Research University Higher School of Economics, Moscow 101000, Russia

³ Faculty of Materials Science, Lomonosov Moscow State University, Moscow 119991, Russia

⁴ Institute of Theoretical and Experimental Biophysics of the Russian Academy of Sciences, Pushchino 142290, Russia

⁵ Frumkin Institute of Physical Chemistry and Electrochemistry of the Russian Academy of Sciences, Moscow 119071, Russia

* Correspondence: van@igic.ras.ru

Abstract: Crystalline cerium(III) phosphate (CePO₄), cerium(IV) phosphates, and nanocrystalline ceria are considered to be promising components of sunscreen cosmetics. This paper reports on a study in which, for the first time, a quantitative comparative analysis was performed of the UV-shielding properties of CePO₄, Ce(PO₄)(HPO₄)_{0.5}(H₂O)_{0.5}, and CePO₄/CeO₂ composites. Both the sun protection factor and protection factor against UV-A radiation of the materials were determined. Ce(PO₄)(HPO₄)_{0.5}(H₂O)_{0.5} was shown to have a sun protection factor of 2.9, which is comparable with that of nanocrystalline ceria and three times higher than the sun protection factor of CePO₄. Composites containing both cerium dioxide and CePO₄ demonstrated higher sun protection factors (up to 1.8) than individual CePO₄. When compared with the TiO₂ Aeroxide P25 reference sample, cerium(III) and cerium(IV) phosphates demonstrated negligible photocatalytic activity. A cytotoxicity analysis performed using two mammalian cell lines, hMSc and NCTC L929, showed that CePO₄, Ce(PO₄)(HPO₄)_{0.5}(H₂O)_{0.5}, and nanocrystalline ceria were all non-toxic. The results of this comparative study indicate that cerium(IV) phosphate Ce(PO₄)(HPO₄)_{0.5}(H₂O)_{0.5} is more advantageous for use in sunscreens than either cerium(III) phosphate or CePO₄/CeO₂ composites, due to its improved UV-shielding properties and low photocatalytic activity.

Keywords: cerium; UV shielding; photocatalytic activity; biocompatibility



Citation: Kozlova, T.O.; Vasilyeva, D.N.; Kozlov, D.A.; Kolesnik, I.V.; Teplonogova, M.A.; Tronev, I.V.; Sheichenko, E.D.; Protsenko, M.R.; Kolmanovich, D.D.; Ivanova, O.S.; et al. A Comparative Study of Cerium(III) and Cerium(IV) Phosphates for Sunscreens. *Molecules* **2024**, *29*, 2157. <https://doi.org/10.3390/molecules29092157>

Academic Editor: Hai-yang Liu

Received: 10 April 2024

Revised: 2 May 2024

Accepted: 3 May 2024

Published: 6 May 2024



Copyright: © 2024 by the authors. Licensee MDPI, Basel, Switzerland. This article is an open access article distributed under the terms and conditions of the Creative Commons Attribution (CC BY) license (<https://creativecommons.org/licenses/by/4.0/>).

1. Introduction

Excessive exposure to sunlight, especially to its ultraviolet component (200–400 nm), has a harmful effect on skin and can lead to premature ageing, erythema, sunburn, and even cancer [1]. To prevent skin damage, it is recommended to use sunscreens containing UV filters—organic or inorganic substances capable of reducing the negative effects of sunlight, due to a combination of various chemical or physical factors [2]. Organic UV filters include various compounds, e.g., cinnamates, avobenzone, octocrylene, salicylates, benzophenones, etc. Despite their diverse chemical composition, organic UV filters share several characteristics that may pose a risk to human health. These include a tendency toward photodegradation under UV light, a proclivity to penetrate the skin barrier and exert a systemic effect on the body, as well as the potential to cause allergic reactions, endocrine disorders, and other issues [3,4]. In contrast, inorganic UV filters possess a higher photostability than organic compounds, lack the ability to penetrate the skin, and are the most recommended in terms of safety for sunscreen applications. Today, the most widely

used inorganic UV filters are titanium dioxide and zinc oxide, which provide protection against solar radiation in a wide spectral range, especially in comparison with organic filters [5]. However, as numerous studies have shown, under certain conditions, these oxides themselves negatively affect the skin, for example, due to the photocatalytic generation of reactive oxygen species, which impart multiple adverse effects [6]. Recently, nanocrystalline cerium dioxide, ceria-based solid solutions, and calcium or cerium phosphates [7–10] have been proposed as safer alternatives to TiO₂ and ZnO materials. Notably, phosphate materials barely interact with organic phosphate-rich compounds that are present in sunscreen formulations, which improves stability and extends the shelf life of the latter [11].

In previous studies regarding cerium phosphates as UV-protective materials, much attention was paid to Ce(III) compounds [12–16], and only a few reports were devoted to Ce(IV) phosphates [17,18] or cerium phosphate composites with CeO₂ [19,20]. All of these materials have been shown to possess a high-enough absorption in the UV range and extremely low photocatalytic activity, which makes them suitable for use in sunscreen cosmetics.

In the present study, to evaluate the performance of cerium-based components of sunscreens, a comparative analysis was conducted of the UV-filter properties of cerium(IV) phosphate, Ce(PO₄)(HPO₄)_{0.5}(H₂O)_{0.5}; cerium(III) phosphate, CePO₄ (monazite); CePO₄/CeO₂ composites; and nanocrystalline CeO₂ (reference sample). The sun protection factor (SPF) and protection factor against UV-A radiation (UVAPF) were selected as quantitative measures, to enable the findings to be comparable with similar studies. This analysis was supplemented by an evaluation of the photocatalytic activity of these materials and their cytotoxicity, to determine the most preferable cerium-based compound for use in sunscreens.

2. Experimental Section

The following materials were used, as received, without further purification: Ce(NO₃)₃·6H₂O (pure grade, Lanhit, Moscow, Russia), phosphoric acid (85 wt.% aq, $\rho = 1.689 \text{ g/cm}^3$, extra-pure grade, Komponent-Reaktiv, Moscow, Russia), sodium hydroxide (high purity grade, Sigma-Aldrich, St. Louis, MO, USA), aqueous ammonia (25 wt.% aq, extra-pure grade, Khimmed, Moscow, Russia), isopropanol (extra-pure grade, Khimmed), and distilled water.

Nanocrystalline CeO₂, which was used for the synthesis of crystalline ceric phosphate Ce(PO₄)(HPO₄)_{0.5}(H₂O)_{0.5} and as a reference sample, was obtained in accordance with the previously published procedure [21]. Briefly, 0.08 M cerium(III) nitrate solution in aqueous isopropanol (water:isopropanol = 1:1 *v/v*) was mixed with 3 M aqueous ammonia. The yellow precipitate obtained was washed with distilled water to a neutral pH and dried at 60 °C. As a second reference sample, CeO₂ annealed at 700 °C for 2 h was used (labelled as CeO₂-700). Crystalline Ce(PO₄)(HPO₄)_{0.5}(H₂O)_{0.5} (hereinafter referred to as CeHP) was synthesised by hydrothermal treatment of ceric phosphate solution at 180 °C for 24 h [22]. Composites of cerium(III) phosphate and ceria (CePO₄/CeO₂) were obtained as reported earlier [22]. Briefly, 1 M NaOH solution (107 mL) was added to 0.16 g of ceric phosphate Ce(PO₄)(HPO₄)_{0.5}(H₂O)_{0.5} and allowed to stand in a closed vessel, with stirring, for 48 or 96 h. Each of the samples obtained was washed several times with distilled water and dried at 60 °C for 24 h in air. Dried products were subjected to thermal treatment in a muffle furnace by linear heating (5 °C/min) to 700 °C or 1000 °C and were kept for 2 h in air (see Figure 1, Table 1). A Ce^{III}PO₄ sample (hereinafter referred to as CeP) was produced by thermal treatment of Ce(PO₄)(HPO₄)_{0.5}(H₂O)_{0.5} at 1000 °C (heating rate 5 °C/min) for 2 h in air.

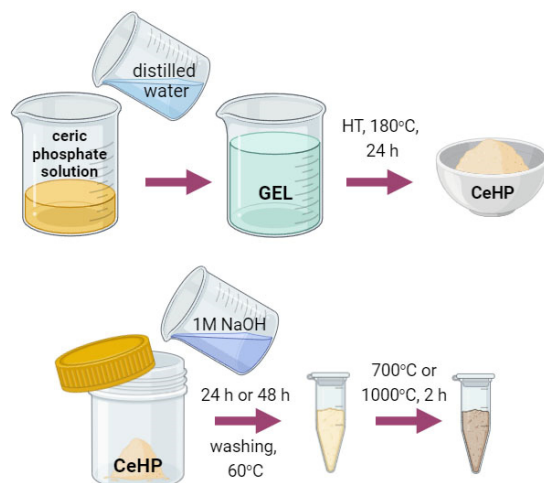


Figure 1. The scheme of the synthesis of ceric phosphate, $\text{Ce}(\text{PO}_4)(\text{HPO}_4)_{0.5}(\text{H}_2\text{O})_{0.5}$, and $\text{CePO}_4/\text{CeO}_2$ composites.

Table 1. Synthesis parameters and designations of the cerium phosphate/ceria composites.

| Sample | C48-700 | C48-1000 | C96-700 | C96-1000 |
|--|---------|----------|---------|----------|
| Soaking duration in 1 M NaOH solution, h | 48 | 48 | 96 | 96 |
| Annealing temperature, °C | 700 | 1000 | 700 | 1000 |

Powder X-ray diffraction (PXRD) patterns were acquired with a DX-2700BH (Haoyuan, Dandong, China) diffractometer, using $\text{Cu K}\alpha_{1,2}$ radiation in the 2θ range of 5° – 80° with 0.02° 2θ steps and a counting time of no less than 0.2 s per step. The identification of the diffraction peaks was carried out using the ICDD database. The full-profile analysis of diffraction patterns, with quantitative determination of the crystal phases ratio and the size of coherent scattering regions, was performed using the Rietveld method and the MAUD software package (version 2.99).

Scanning electron microscopy (SEM) images were obtained using an Amber GMH (Tescan, Brno, Czech Republic) or an NVision 40 (Carl Zeiss, Oberkochen, Germany) microscope, operated at an accelerating voltage of 1 kV using an Everhart–Thorney secondary electron detector or a backscattered electron InLens detector. Energy-dispersive X-ray spectroscopy (EDX) data were obtained using an Ultim Max (Oxford Instruments, Abingdon, UK) detector at an accelerating voltage of 20 kV.

Fourier-transform infrared (FTIR) spectra of the samples were recorded using an InfraLUM FT-08 (Lumex, St. Petersburg, Russia) spectrometer in the range of 400 – 4000 cm^{-1} in attenuated total reflectance mode.

Raman spectra were obtained using a Confotech NR-500 spectrometer (SOL Instruments, Minsk, Belarus) with 532 nm laser excitation using $20\times$ objective ($\text{NA} = 0.45$) at $\sim 2\text{ mW}$ laser power.

Absorption spectra of CeO_2 , CeHP, CeP, and $\text{CePO}_4/\text{CeO}_2$ composites were registered in a diffuse reflection mode on a Lambda 950 (PerkinElmer, Waltham, MA, USA) spectrometer in the 200 – 1000 nm range. The SPF and UVAPF values were determined in accordance with the ISO 24443-2016 international standard [23], which implies the possibility of establishing the values of sun protection factors that correlate with in vivo changes, using spectral measurements in vitro and mathematical modelling. The measurement procedure and calculation formulae have been reported elsewhere [18]. Sample preparation for this study included the following steps: 10 wt.% suspensions containing 0.06 g of cerium phosphates, or composites, or CeO_2 powders and 0.54 g of a solution consisting of 9.9 wt.% H_2O , 90 wt.% glycerol, and 0.1 wt.% sodium dodecyl sulfate were prepared

in an agate mortar and used for further analysis; 0.035 g of each suspension was evenly spread over the surface of the 3M Transpore Tape 1527-2 film (27.5 cm² area). The total transmittance spectra of the films coated with the suspensions were recorded on a Lambda 950 (PerkinElmer, Waltham, MA, USA) spectrometer using an integrating sphere (150 mm diameter) in the range of 290–400 nm; 3M Transpore Tape 1527-2 coated with a similar formulation, with neither cerium phosphates nor other cerium-containing materials, was used as a reference sample. For each material, measurements were repeated at least four times, using similarly prepared tapes, and then averaging the resulting values. A Suntest CPS+ (ATLAS MTS, Linsengericht, Germany) device was used as a source of UV radiation.

The photocatalytic degradation of methylene blue under UV–visible light irradiation was chosen as a model reaction to assess the photocatalytic activity of the samples. An HPX-2000 (OceanOptics, Orlando, FL, USA) xenon lamp was used as the light source. In a typical experiment, 1 mg of the sample was dispersed in 2 mL of deionised water and the mixture was stirred for 30 min ($t = 37\text{ }^{\circ}\text{C}$). Then, 0.1 mL of 100 mg/L methylene blue (MB) solution was added and the suspension obtained was stirred for 45 min in the dark. The suspension was subsequently irradiated for 4 h and the concentration of MB was monitored by registering UV–visible spectra every minute, using an QE65000 (OceanOptics, Orlando, FL, USA) spectrometer. The kinetics of methylene blue degradation was described by a first-order equation and photocatalytic activity was determined as the decomposition rate constant normalised to the photocatalyst's weight. Commercial photocatalyst TiO₂ Aeroxide P25 (Evonik, Essen, Germany) was used as a reference sample.

Since the cytotoxicity of CeP and nanocrystalline CeO₂ powders had been recently assessed [18], here, a similar study was performed for the Ce^{III}PO₄ sample using cell cultures of human mesenchymal stem cells and line NCTC L929 mouse fibroblasts. The cells were seeded in 96-well plates at a density of 20,000 cells/cm² in a DMEM/F12 culture medium containing 10% fetal bovine serum. After 12 h of cultivation, the nutrient medium was replaced with an identical medium containing Ce^{III}PO₄ suspended in the medium, using a magnetic stirrer for 30 min. The concentrations of Ce^{III}PO₄ in DMEM/F12 medium were 0.125 mg/mL, 0.25 mg/mL, 0.5 mg/mL, and 1 mg/mL. In a control experiment, the culture medium was replaced with a fresh medium that did not contain cerium(III) phosphate.

The MTT test was used to assess the viability of the cells. After 48 h, the nutrient medium with Ce^{III}PO₄ was replaced with a serum-free culture medium DMEM/F12 containing tetrazolium salt at a concentration of 0.5 mg/mL. After incubation of the plate for 3 h at 37 °C (5% CO₂), the culture medium was removed and 100 µL of DMSO was added. The plates were shaken, at room temperature, for 10 min (200 rpm) to dissolve the formazan crystals. The optical density of formazan was measured on a BIO-RAD 680 photometer at 540 nm. Statistical data processing was performed using GraphPad Prism 8 software. Statistically significant differences were determined in accordance with the Mann–Whitney U-test.

The differential staining of human mesenchymal stem cells using fluorescent dyes SYTO 9 (green) and propidium iodide (red) was used to assess the proportion of dead cells. During the experiment, the dyes were dissolved in Hanks' balanced salt solution (HBSS). Cells were stained using a dye concentration of 5 µM. Then, the cells were incubated for 15 min at 37 °C in a humidified atmosphere (5% CO₂) and images were taken using a Zeiss 200 M inverted fluorescence microscope. The micrographs were further processed using ImageJ software (version 1.53i).

3. Results and Discussion

The powders obtained differed in colour: yellow grey (CeHP), yellow and brown yellow (initial ceria, CeO₂-700, C48-700, and C96-700 samples), grey beige (C48-1000, and C96-1000 composites) and white grey (CeP), as illustrated in Figure 2. Note that, for cosmetic applications, it is strongly recommended to use UV filters with a natural appearance of skin [24].

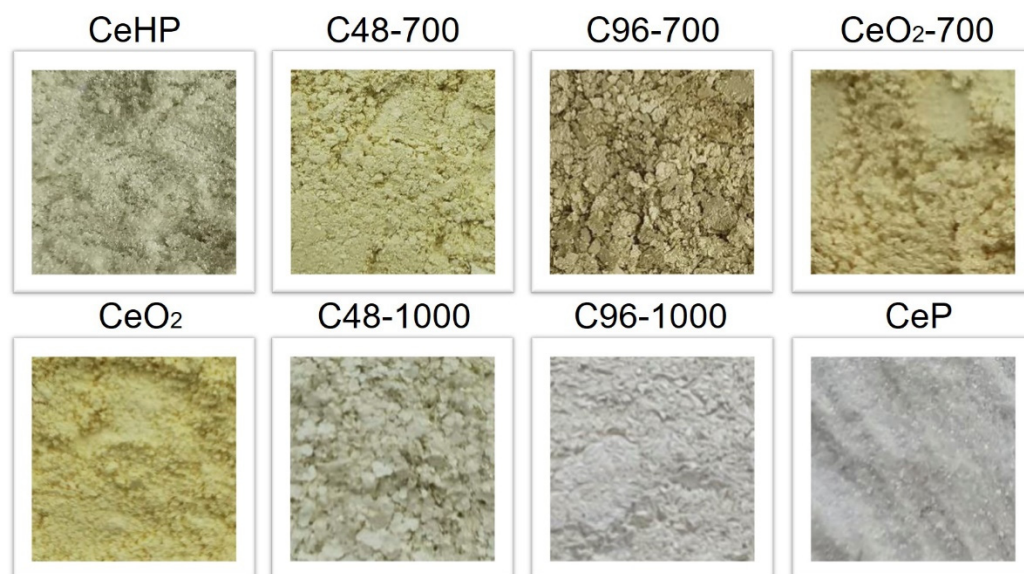


Figure 2. Appearance of ceria, cerium phosphates, and $\text{CePO}_4/\text{CeO}_2$ composites (optical images).

According to the X-ray diffraction data (Figure 3), the reference ceria samples (CeO_2 , and CeO_2 -700) and CeHP were a single-phase cerium dioxide (ICDD 34-0394) and $\text{Ce}(\text{PO}_4)(\text{HPO}_4)_{0.5}(\text{H}_2\text{O})_{0.5}$ [25], respectively. The CeP sample was a highly textured CePO_4 (monazite, ICDD 32-199) with a small (4.1 ± 0.3 wt.%) admixture of CeP_3O_9 (ICDD 33-0336). This minor admixture would not significantly affect the absorbance spectrum of the product (CeP_3O_9 band gap is nearly 6 eV [26]), so any differences changes in its SPF value compared with pure CePO_4 are expected to be negligible. Samples C48-700, C48-100, C96-700, and C96-1000 contained a mixture of CeO_2 and CePO_4 with various crystal phase ratios (see Table 2). An increase in the annealing temperature from 700 °C to 1000 °C led to a significant increase in ceria particle sizes in composites, from ten nanometres to more than 100 nanometres. At the same time, the duration of CeHP alkaline hydrolysis (48 or 96 h) had virtually no effect on the phase composition and crystallite sizes of the composites.

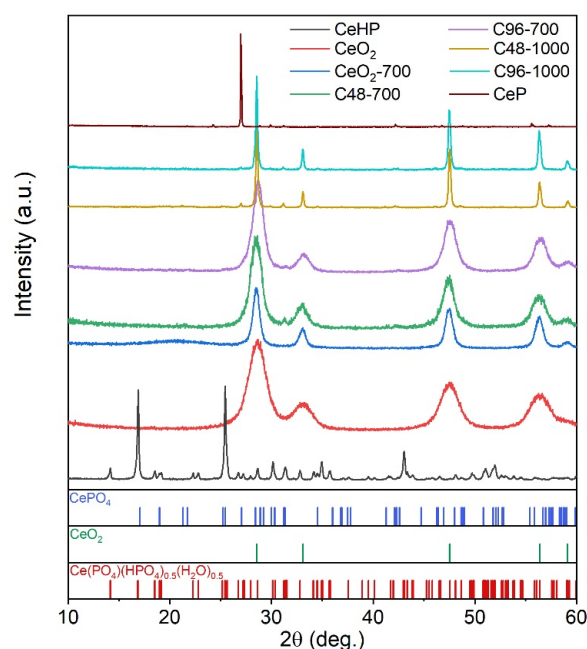


Figure 3. Diffraction patterns of ceria, cerium phosphates, and $\text{CePO}_4/\text{CeO}_2$ composites.

Table 2. Structural parameters and crystallite sizes of ceria, cerium phosphates, and composites samples obtained by XRD analysis.

| Sample | Phase Composition | Lattice Parameters | Crystallite Size, nm |
|-----------------------|--|--|---|
| CeO ₂ | CeO ₂ : 100 wt.% | $a = 5.4184(7) \text{ \AA}$ | 6.2 ± 0.5 |
| CeO ₂ -700 | CeO ₂ : 100 wt.% | $a = 5.4121(7) \text{ \AA}$ | 16.4 ± 0.5 |
| CeHP | Ce(PO ₄)(HPO ₄) _{0.5} (H ₂ O) _{0.5} : 100 wt.% | $a = 21.041(1) \text{ \AA}$ $b = 6.5644(5) \text{ \AA}$ $c = 6.9609(5) \text{ \AA}$ $\beta = 91.965(5)^\circ$ | >100 |
| CeP | CePO ₄ : 96.1 ± 2.9 wt. % CeP ₃ O ₉ : 4.1 ± 0.3 wt. % | CePO ₄ : $a = 6.7969(2) \text{ \AA}$ $b = 7.0202(6) \text{ \AA}$ $c = 6.4689(5) \text{ \AA}$ $\beta = 103.453(4)^\circ$ CeP ₃ O ₉ : $a = 11.28(1) \text{ \AA}$ $b = 8.60(1) \text{ \AA}$ $c = 7.345(1) \text{ \AA}$ | >100 |
| C48-700 | CeO ₂ : 94.3 ± 0.6 wt. % CePO ₄ : 5.7 ± 0.2 wt. % | CeO ₂ : $a = 5.4166(7) \text{ \AA}$ CePO ₄ : $a = 6.756(5) \text{ \AA}$ $b = 6.956(5) \text{ \AA}$ $c = 6.444(4) \text{ \AA}$ $\beta = 103.83(7)^\circ$ | CeO ₂ : 9.7 ± 0.5 CePO ₄ : 80 ± 30 |
| C48-1000 | CeO ₂ : 82.5 ± 0.7 wt. % CePO ₄ : 17.4 ± 0.7 wt. % | CeO ₂ : $a = 5.4116(2) \text{ \AA}$ CePO ₄ : $a = 6.793(1) \text{ \AA}$ $b = 7.019(1) \text{ \AA}$ $c = 6.469(1) \text{ \AA}$ $\beta = 103.46(1)^\circ$ | CeO ₂ : >100 CePO ₄ : >100 |
| C96-700 | CeO ₂ : 100 wt. % CePO ₄ : not detected | $a = 5.419(1) \text{ \AA}$ | 9.9 ± 0.5 |
| C96-1000 | CeO ₂ : 85.6 ± 0.9 wt. % CePO ₄ : 14.3 ± 1.0 wt. % | CeO ₂ : $a = 5.4125(2) \text{ \AA}$ CePO ₄ : $a = 6.786(2) \text{ \AA}$ $b = 7.021(3) \text{ \AA}$ $c = 6.467(2) \text{ \AA}$ $\beta = 103.36(3)^\circ$ | CeO ₂ : >100 CePO ₄ : >100 |

IR spectra of cerium(III) and cerium(IV) phosphates, as well as CePO₄/CeO₂ composites, are presented in Figure 4. The IR spectrum of the CeHP sample coincides well with the Ce(PO₄)(HPO₄)_{0.5}(H₂O)_{0.5} spectrum [27,28] and comprises two major absorption bands at 1100–900 cm⁻¹ and 650–440 cm⁻¹, which correspond to the stretching and deformational vibrations of the phosphate anion, respectively [29]. In the IR spectrum of the CeP sample, in addition to the characteristic absorption bands of the phosphate anions [30], there are two weak absorption bands, at 1270 cm⁻¹ and 770 cm⁻¹, which can be attributed to metaphosphate group vibrations [31,32]. The presence of characteristic absorption bands at 1100–900 cm⁻¹ and 650–440 cm⁻¹ in the IR spectrum of the C96-700 composite indicates phosphate anions and indirectly confirms the formation of a CePO₄ admixture, which was not detected by XRD analysis.

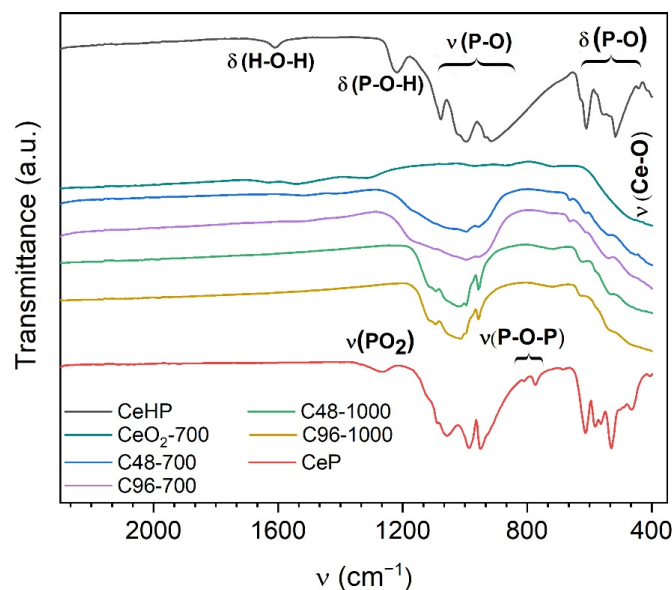


Figure 4. IR spectra of CeO₂, cerium phosphates, and composite samples.

The presence of the absorption band at 468 cm^{-1} in the Raman spectra of ceria samples and CePO₄/CeO₂ composites (Figure 5) is definitely associated with the F_{2g} band of CeO₂ [33]. The characteristic peak at 464 cm^{-1} in the spectra of CePO₄/CeO₂ composites is narrower and more symmetrical than in the spectrum of pure ceria, while its half-width decreases with increasing annealing temperature. The observed trend was caused by an increase in the size of CeO₂ crystallites [34], which was confirmed by XRD data. The broad band at $550\text{--}600\text{ cm}^{-1}$ observed in the spectra of ceria powder, C48-700, and C96-700 composites could be due to the oxygen defects in CeO₂ nanocrystals [35]. The peak observed at 970 cm^{-1} confirms the presence of phosphate groups in the composites [29].

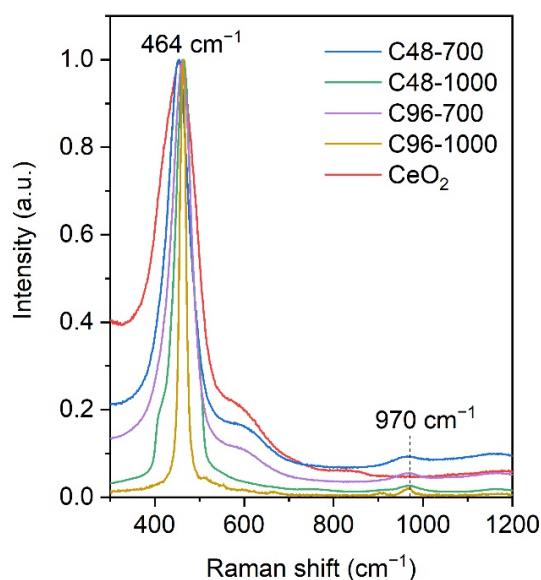


Figure 5. Raman spectra of ceria and composite samples.

Scanning electron microscopy data for the CeHP sample and its thermolysis products, including CePO₄/CeO₂ composites, are presented in Figure 6. CeHP, C48-700, and C96-700 samples consist of lamellar aggregates. Such a microstructure of inorganic UV filters, according to Sato et al. [36], ensures comfort when applying sun protection products to the skin. Powders obtained at $1000\text{ }^{\circ}\text{C}$ consisted of aggregated grains forming a lamellar motif.

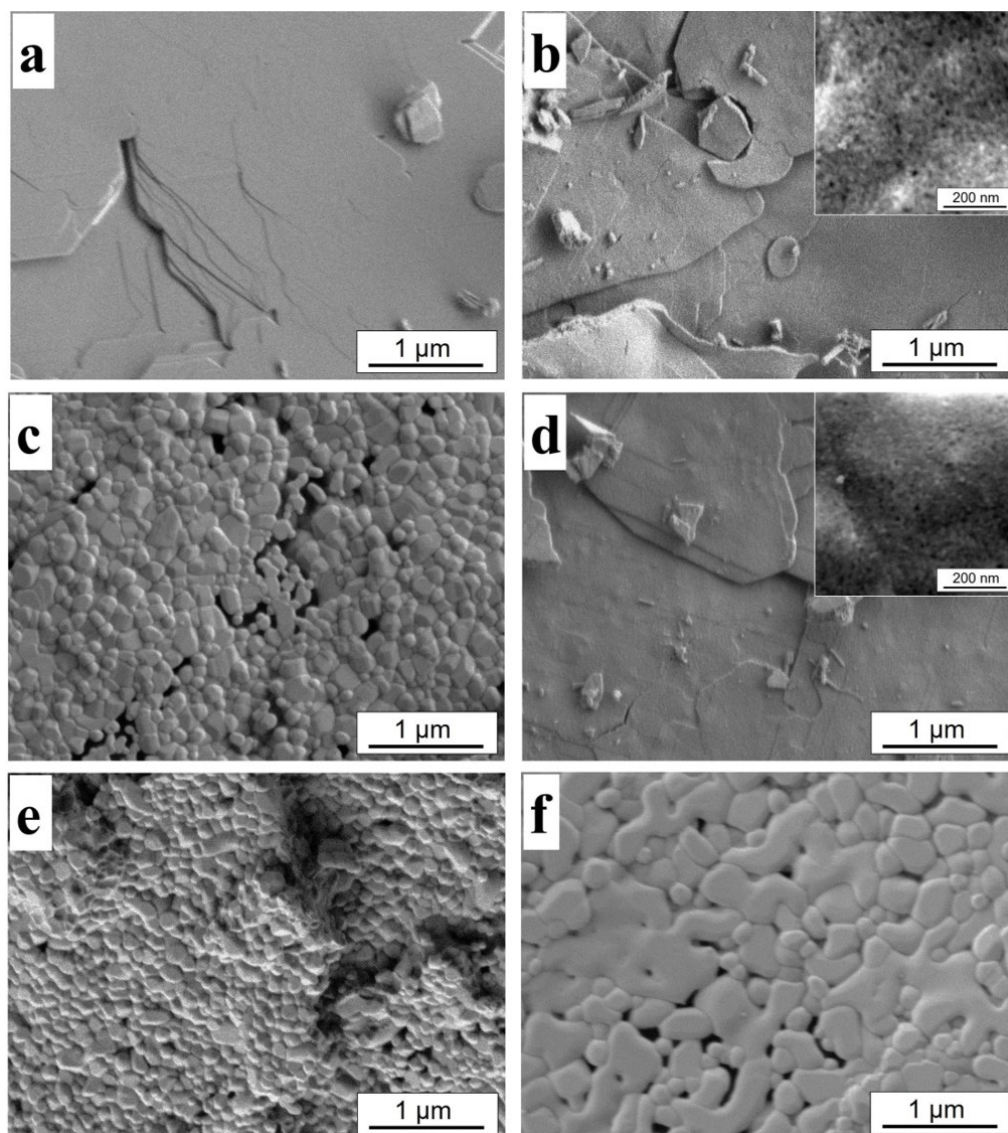


Figure 6. SEM images of (a) CeHP, (b) C48-700, (c) C48-1000, (d) C96-700, (e) C96-1000, and (f) CeP samples.

EDX data show that the Ce:P ratio for the CeHP and CeP samples was close to the nominal compositions (1:1.5 and 1:1, respectively). For all the composites, the presence of phosphorus was detected, with the content of cerium being approximately seven times higher than that of phosphorus (Table S1, Supplementary Materials). This additionally confirms the formation of cerium dioxide in the composites.

The distribution of phases in the obtained composites was studied using SEM-EDX mapping (Figure 7). In the sample heated at 700 °C, cerium, phosphorus, and oxygen are uniformly distributed in the lamellar particles of the composites. For the sample heated at 1000 °C, the SEM images taken at the backscattered electron mode show that, on the surface of the lamellar particles, the bright particles with a higher average atomic number are present, most likely cerium oxide. The dark areas in the corresponding SEM images show a higher phosphorus content (see EDX maps), while cerium and oxygen are uniformly distributed. It can, therefore, be concluded that, on the phosphate surface, the formation of CeO₂ nanoparticles occurs after etching in aqueous NaOH and subsequent treatment at 700 °C. At 1000 °C, relatively large CeO₂ particles form on the surface of phosphate-rich lamellar aggregates, which consist of crystalline monazite.

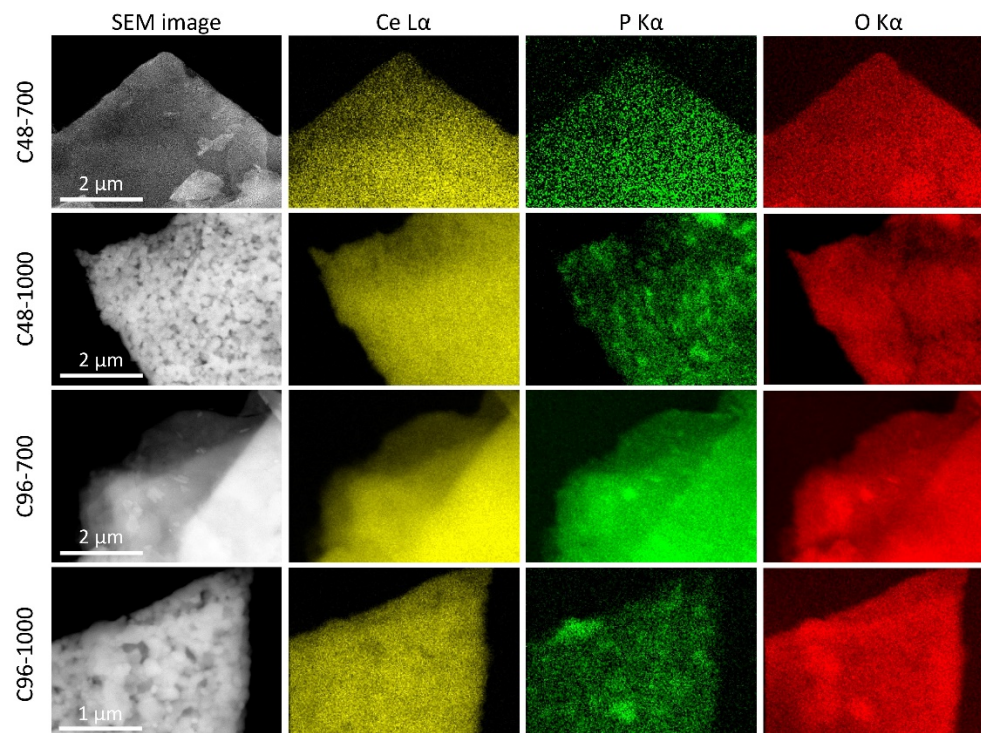


Figure 7. SEM images in the backscattered electron mode for the $\text{CePO}_4/\text{CeO}_2$ composites and corresponding EDX maps of cerium (yellow), phosphorous (green), and oxygen (red).

The UV–vis absorption spectra of the powders (Figure S1) show the characteristic wide bands below 400 nm for the ceria and CeHP samples, as well as for the CeP sample, corresponding to charge-transfer transitions between the $\text{O}(2p)$ and $\text{Ce}(4f)$ states [37,38] or the $4f^1-5d^1$ electron transition of Ce^{+3} [39,40], respectively. For the $\text{CePO}_4/\text{CeO}_2$ composites, the absorption spectra virtually coincide with the corresponding spectrum of the CeO_2 sample, while, in the composites, a slight shift in the absorption band edge can be observed, apparently due to the presence of Ce^{+3} and structural defects [41–46].

According to the ISO 24443-2016 international standard [23] for the correct SPF and UVAPF determination, the absorption spectra of suspensions containing UV filters should be registered a few times, just before, and just after their irradiation with UV light. Figure 8 shows the averaged UV–vis absorption spectra of suspensions containing cerium dioxide samples, CeHP, CeP, and $\text{CePO}_4/\text{CeO}_2$ composites after UV irradiation. The suspension containing CeP powder demonstrated the lowest absorption values, in the range of 290–400 nm, while CeHP and nanocrystalline CeO_2 possessed the highest absorption. The absorption values of the suspensions containing $\text{CePO}_4/\text{CeO}_2$ composites were lower than the absorption of CeO_2 -700-containing suspension. Suspensions containing C48-700 and C96-700 composites showed a greater absorption than the corresponding suspensions containing the composites annealed at 1000 °C. The calculated values of the sun protection factor for the samples were directly dependent on the absorbance of their suspension, ranging from 2.9 for CeHP and nanocrystalline ceria (which is close to the previously published data [18,47]) to 1.0 for CeP (see Table 3). Both nanocrystalline ceria and CeHP also demonstrated the highest protection factor against UV-A radiation.

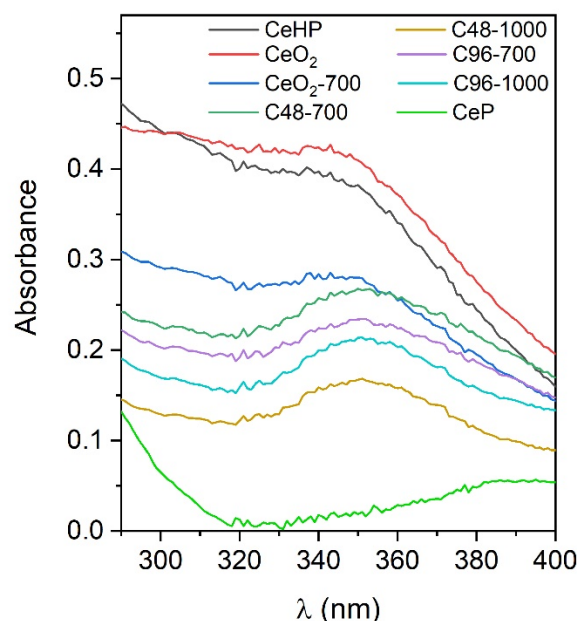


Figure 8. Averaged UV-vis absorption spectra of the suspensions containing ceria, cerium phosphates, and $\text{CePO}_4/\text{CeO}_2$ composites.

Table 3. Sun protection factor, UV-A protection factor, and critical wavelength values for the samples of ceria, cerium phosphates, and $\text{CePO}_4/\text{CeO}_2$ composites.

| Sample | SPF | UVAPF | UVAPF/SPF | λ_{crit} , nm |
|---------------------------------|-----|-------|-----------|------------------------------|
| CeHP | 2.9 | 2.5 | 0.9 | 381 |
| CeO_2 | 2.9 | 2.7 | 0.9 | 382 |
| CeO_2 -700 | 2.0 | 1.9 | 1.0 | 383 |
| C48-700 | 1.8 | 1.8 | 1.0 | 386 |
| C96-700 | 1.7 | 1.7 | 1.0 | 385 |
| C48-1000 | 1.4 | 1.4 | 1.0 | 385 |
| C96-1000 | 1.5 | 1.5 | 1.0 | 386 |
| CeP | 1.0 | 1.0 | 1.0 | 395 |
| TiO_2 (anatase) [18] | 2.7 | 2.5 | 0.9 | |
| TiO_2 (anatase) [18] | 3.1 | 3.1 | 1.0 | |
| ZnO (Z-Cote [®]) [47] | 3.7 | 3.8 | 1.0 | |

In addition, the suspensions were assessed in terms of the critical wavelength (λ_{crit}) and UVAPF/SPF values. For all samples, these values exceeded the minimum threshold value of 370 nm and 1/3, respectively [48].

Inorganic components of sunscreen cosmetics, in addition to high SPF values, should also possess low photocatalytic activity (PCA). Thus, an assessment was made of the rate of methylene blue dye photodegradation in the presence of CeHP, CeP, CeO_2 , and C48-700 samples (the latter has one of the highest SPF values among the $\text{CePO}_4/\text{CeO}_2$ composites), in comparison with commercial titanium dioxide (Aeroxide TiO_2 P25).

Figure 9 shows that the CeP sample, having the lowest SPF value, did not possess any photocatalytic activity, which correlates well with previous reports [12,36,49]. Both ceria and CeHP samples provided almost the same rate of methylene blue photodegradation, which was approximately ten times lower than the corresponding value for TiO_2 . The low level of photocatalytic activity of nanocrystalline ceria compared with titanium dioxide is also in line with previous reports [50–54]. At the same time, the C48-700 composite

showed a higher photocatalytic performance than CeO_2 , which can be caused by the complex interplay of several factors, such as the particle morphology, particle size, lifetime of photogenerated electron-hole pairs [55], redox switching between Ce^{+3} and Ce^{+4} in $\text{CePO}_4/\text{CeO}_2$ composites [56–58], etc.

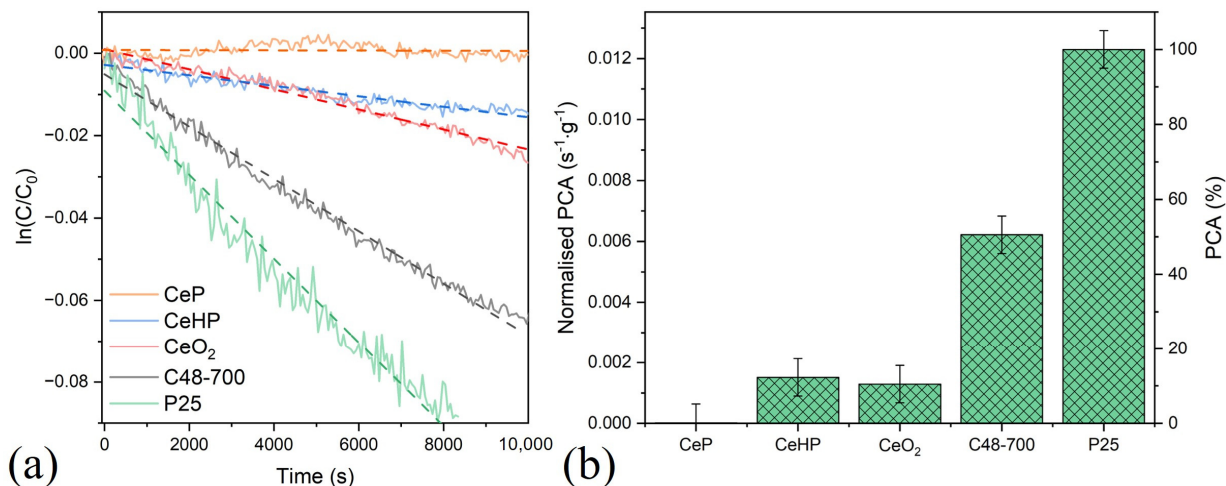


Figure 9. (a) Kinetic curves of methylene blue dye photodegradation in the presence of CeP, CeHP, C48-700, ceria, and TiO_2 Aeroxide TiO_2 P25 samples; and (b) normalised photocatalytic activity (PCA) for the corresponding samples.

As shown previously, cerium(IV) compounds—ceria and ceric phosphate $\text{Ce}(\text{PO}_4)(\text{HPO}_4)_{0.5}(\text{H}_2\text{O})_{0.5}$ —are non-toxic to mammalian cell cultures, which potentially allow them to be considered to be promising components of sunscreen cosmetics [18]. In the present study, $\text{Ce}^{\text{III}}\text{PO}_4$ cytotoxicity was analysed under similar conditions, in order to make the comparison of cerium(III) and (IV) phosphates more detailed.

The results of the MTT test for human mesenchymal stem cells and NCTC L929 mouse fibroblasts (Figure 10) showed no significant differences between the CeHP [18] and CeP samples, indicating the absence of the toxic effect in the concentration range of 0.125–1 mg/mL. The results of the live/dead assay (Figure 11) are consistent with the MTT test data.

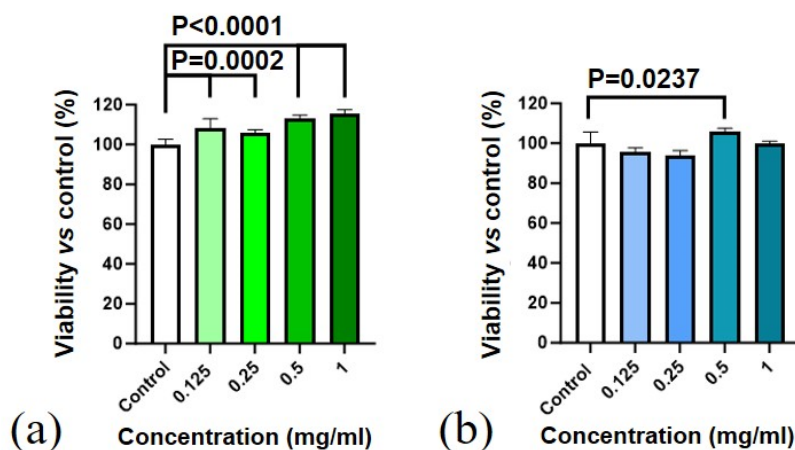


Figure 10. Metabolic activity of (a) human mesenchymal stem cells and (b) mouse fibroblasts of the NCTC L929 line after 48 h of cultivation with the CeP sample in concentrations of 1, 0.5, 0.25, and 0.125 mg/mL. Seeding density was $20,000\text{ cm}^{-2}$. $M \pm \text{SD}$, Mann–Whitney U-test, at $p = 0.05$.

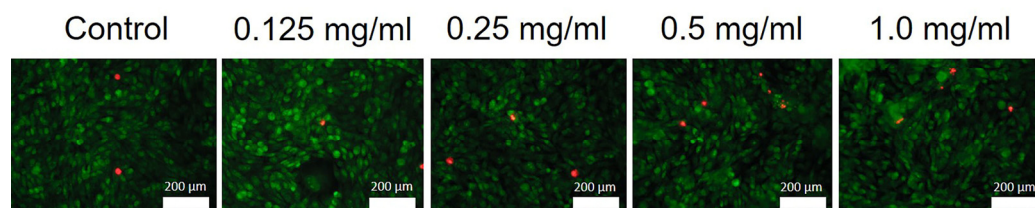


Figure 11. Appearance of L929 mouse fibroblasts in the presence of the CeP sample. Images were taken at 200× magnification. Scale bar—200 µm. SYTO 9 and propidium iodide dyes (live/dead test) were used. Green—live cells, red—dead cells.

Although the data on the toxicity of cerium(III) ions had already been reported [59–61], the low toxicity of the CePO_4 was apparently due to the extremely low solubility of monazite [62–64] and the absence of free cerium ions in the solution. When comparing cerium phosphates and cerium dioxide, some disadvantages of ceria should be taken into account. In particular, its pro-oxidant activity at the natural pH of the skin (~5) has been reported earlier, as well as the tendency to interact with phosphate groups of sunscreen components or cell membranes [65–68]. Biocompatibility and stability in the biological environment of the phosphate matrix make cerium phosphates the most promising candidates for use in sunscreen cosmetics; they are free from the abovementioned limitations inherent in ceria.

4. Conclusions

This paper presents a first comparative quantitative assessment of the UV-shielding properties (SPF, UVAPF, λ_{crit}) of cerium(III) and (IV) phosphates, as well as $\text{Ce}^{\text{III}}\text{PO}_4/\text{Ce}^{\text{IV}}\text{O}_2$ composites. It has been shown that $\text{Ce}(\text{PO}_4)(\text{HPO}_4)_{0.5}(\text{H}_2\text{O})_{0.5}$ and CePO_4 (monazite) powders, with a similar crystallite size and lamellar microstructure, have SPF values of 2.9 (like nanocrystalline ceria) and 1.0, respectively. Composites containing CeO_2 and CePO_4 phases have SPF values between 1.4 and 1.8, which exceed the corresponding value for the individual CePO_4 (monazite). At the same time, CePO_4 powder has no photocatalytic activity in the reaction of methylene blue degradation. The photocatalytic activity of $\text{Ce}(\text{PO}_4)(\text{HPO}_4)_{0.5}(\text{H}_2\text{O})_{0.5}$ is comparable with the photocatalytic activity of nanocrystalline ceria, being ten times lower than that of Aeroxide TiO_2 P25. The $\text{Ce}^{\text{III}}\text{PO}_4/\text{Ce}^{\text{IV}}\text{O}_2$ composite with SPF 1.8 possesses the highest photocatalytic activity, which is only half that of Aeroxide TiO_2 P25. The absence of cytotoxicity of CePO_4 towards human mesenchymal stem cells and NCTC L929 mouse fibroblasts has been demonstrated by MTT and live/dead tests. Based on the whole body of data obtained, $\text{Ce}(\text{PO}_4)(\text{HPO}_4)_{0.5}(\text{H}_2\text{O})_{0.5}$ is concluded to be the most promising sunscreen component among the cerium-containing materials studied.

Supplementary Materials: The following supporting information can be downloaded at: <https://www.mdpi.com/article/10.3390/molecules29092157/s1>, Figure S1: Normalised UV-vis absorption spectra of ceria, cerium phosphates and $\text{CePO}_4/\text{CeO}_2$ composites; Table S1: EDX data for the cerium phosphate/ceria composites.

Author Contributions: Conceptualization, T.O.K. and V.K.I.; methodology, T.O.K. and I.V.K.; validation, D.D.K.; formal analysis, D.A.K. and D.D.K.; investigation, D.N.V., D.A.K., I.V.K., M.A.T., I.V.T., E.D.S., M.R.P., D.D.K. and O.S.I.; data curation, T.O.K., D.A.K. and O.S.I.; writing—original draft, T.O.K.; writing—review and editing, A.E.B. and V.K.I.; supervision, I.V.K., A.E.B. and V.K.I.; funding acquisition, T.O.K. All authors have read and agreed to the published version of the manuscript.

Funding: This research was funded by the Russian Science Foundation grant number 23-73-10088, <https://rscf.ru/en/project/23-73-10088/> (accessed on 2 May 2024).

Institutional Review Board Statement: The in vitro experiments were performed in agreement with good clinical practice and the ethical principles of the current edition of the Declaration of Helsinki, after the permission of the Ethics Committee of the Institute of Theoretical and Experimental

Biophysics of the Russian Academy of Sciences (Puschino, Moscow region, Russian Federation), protocol No. 35 on 5 March 2022. Postnatal human dental pulp stem cells were extracted from the third molar tooth of a 12-year-old human donor. The tooth was removed according to the orthodontic indications of the dental clinic «Dr. MUN» (Moscow, Russia), in accordance with the ethics committee, after consent was signed by the patient's parents. All the experiments were carried out in agreement with good clinical practice and the ethical principles of the current edition of the Declaration of Helsinki. NCTC L929 mouse fibroblasts from the cryobank of the Theranostics and Nuclear Medicine Laboratory (Institute of Theoretical and Experimental Biophysics of the Russian Academy of Sciences (Puschino, Moscow region, Russian Federation) were used.

Informed Consent Statement: Informed consent was obtained from all subjects involved in the study.

Data Availability Statement: Data are contained within the article and Supplementary Materials.

Conflicts of Interest: The authors declare no conflict of interest.

References

1. Gallagher, R.P.; Lee, T.K. Adverse Effects of Ultraviolet Radiation: A Brief Review. *Prog. Biophys. Mol. Biol.* **2006**, *92*, 119–131. [[CrossRef](#)] [[PubMed](#)]
2. Serpone, N.; Dondi, D.; Albini, A. Inorganic and Organic UV Filters: Their Role and Efficacy in Sunscreens and Suncare Products. *Inorganica Chim. Acta* **2007**, *360*, 794–802. [[CrossRef](#)]
3. Ballestín, S.S.; Bartolomé, M.J.L. Toxicity of Different Chemical Components in Sun Cream Filters and Their Impact on Human Health: A Review. *Appl. Sci.* **2023**, *13*, 712. [[CrossRef](#)]
4. Gilbert, E.; Piro, F.; Bertholle, V.; Roussel, L.; Falson, F.; Padois, K. Commonly used UV filter toxicity on biological functions: Review of last decade studies. *Int. J. Cosmet. Sci.* **2013**, *35*, 208–219. [[CrossRef](#)] [[PubMed](#)]
5. González, S.; Fernández-Lorente, M.; Gilaberte-Calzada, Y. The Latest on Skin Photoprotection. *Clin. Dermatol.* **2008**, *26*, 614–626. [[CrossRef](#)] [[PubMed](#)]
6. Kolesnik, I.V.; Aslandukov, A.N.; Arkhipin, A.S.; Kozlov, D.A. Hydrothermal Synthesis of Layered Titanium Phosphate $\text{Ti}_2\text{O}_2\text{H}(\text{PO}_4)[(\text{NH}_4)_2\text{PO}_4]_2$ and Its Potential Application in Cosmetics. *Crystals* **2019**, *9*, 332. [[CrossRef](#)]
7. Egambaram, O.P.; Kesavan Pillai, S.; Ray, S.S. Materials Science Challenges in Skin UV Protection: A Review. *Photochem. Photobiol.* **2020**, *96*, 779–797. [[CrossRef](#)]
8. Carella, F.; Degli Esposti, L.; Adamiano, A.; Iafisco, M. The Use of Calcium Phosphates in Cosmetics, State of the Art and Future Perspectives. *Materials* **2021**, *14*, 6398. [[CrossRef](#)] [[PubMed](#)]
9. Parwaiz, S.; Khan, M.M.; Pradhan, D. CeO_2 -Based Nanocomposites: An Advanced Alternative to TiO_2 and ZnO in Sunscreens. *Mater. Express* **2019**, *9*, 185–202. [[CrossRef](#)]
10. Nery, É.M.; Martínez, R.M.; Velasco, M.V.R.; Baby, A.R. A Short Review of Alternative Ingredients and Technologies of Inorganic UV Filters. *J. Cosmet. Dermatol.* **2021**, *20*, 1061–1065. [[CrossRef](#)]
11. Seixas, V.C.; Serra, O.A. Stability of Sunscreens Containing CePO_4 : Proposal for a New Inorganic UV Filter. *Molecules* **2014**, *19*, 9907–9925. [[CrossRef](#)]
12. De Lima, J.F.; Serra, O.A. Cerium Phosphate Nanoparticles with Low Photocatalytic Activity for UV Light Absorption Application in Photoprotection. *Dye. Pigment.* **2013**, *97*, 291–296. [[CrossRef](#)]
13. Lima, J.F.; De Sousa Filho, P.C.; Serra, O.A. Single Crystalline Rhabdophane-Type CePO_4 Nanoparticles as Efficient UV Filters. *Ceram. Int.* **2016**, *42*, 7422–7431. [[CrossRef](#)]
14. Onoda, H.; Tanaka, R. Synthesis of Cerium Phosphate White Pigments from Cerium Carbonate for Cosmetics. *J. Mater. Res. Technol.* **2019**, *8*, 5524–5528. [[CrossRef](#)]
15. Onoda, H.; Iwashita, M. Synthesis of Novel White Pigments by Shaking Cerium Compounds with Phosphoric Acid. *Emergent Mater.* **2023**, *6*, 1089–1095. [[CrossRef](#)]
16. Masui, T.; Tategaki, H.; Furukawa, S.; Imanaka, N. Synthesis and Characterization of New Environmentally-Friendly Pigments Based on Cerium Phosphate. *J. Ceram. Soc. Jpn.* **2004**, *112*, 646–649. [[CrossRef](#)]
17. Sato, T.; Sato, C.; Yin, S. Optimization of Hydrothermal Synthesis of Plate-Like Hydrated Cerium Phosphates and Their Photochemical Properties. *Phosphorus Res. Bull.* **2008**, *22*, 17–21. [[CrossRef](#)]
18. Kozlova, T.O.; Popov, A.L.; Kolesnik, I.V.; Kolmanovich, D.D.; Baranchikov, A.E.; Shcherbakov, A.B.; Ivanov, V.K. Amorphous and Crystalline Cerium(IV) Phosphates: Biocompatible ROS-Scavenging Sunscreens. *J. Mater. Chem. B* **2022**, *10*, 1775–1785. [[CrossRef](#)]
19. Muthukumar Sivaraman, R.; Daphne Jacinth Gracia, K.; Sheeba Thavamani, S.; Peter Amaladhas, T.; Devanesan, S.; AlSalhi, M.S.; Asemi, N.N.; Natarajan, S. CeO_2 - CePO_4 and Ag@CeO_2 - CePO_4 Nanocomposites from *Penaeus Semisulcatus* for Heavy Metals Sensing, UV Shielding and Cytotoxic Applications. *Arab. J. Chem.* **2024**, *17*, 105382. [[CrossRef](#)]
20. Yin, S.; Saito, M.; Liu, X.; Sato, T. Preparation and Characterization of Plate-like Cerium Phosphate/Nanosize Calcia Doped Ceria Composites by Precipitation Method. *Phosphorus Res. Bull.* **2011**, *25*, 68–71. [[CrossRef](#)]
21. Ivanov, V.K.; Baranchikov, A.E.; Polezhaeva, O.S.; Kopitsa, G.P.; Tretyakov, Y.D. Oxygen Nonstoichiometry of Nanocrystalline Ceria. *Russ. J. Inorg. Chem.* **2010**, *55*, 325–327. [[CrossRef](#)]

22. Kozlova, T.O.; Vasil'eva, D.N.; Kozlov, D.A.; Teplonogova, M.A.; Birichevskaya, K.V.; Baranchikov, A.E.; Gavrikov, A.V.; Ivanov, V.K. On the Chemical Stability of $\text{Ce}^{\text{IV}}(\text{PO}_4)(\text{HPO}_4)_{0.5}(\text{H}_2\text{O})_{0.5}$ in Alkaline Media. *Russ. J. Inorg. Chem.* **2022**, *67*, 1901–1907. [[CrossRef](#)]
23. ISO 24443; Determination of Value Sunscreen UVA Protection Factor In Vitro. International Organization for Standardization: Geneva, Switzerland, 2016.
24. Lyons, A.B.; Trullas, C.; Kohli, I.; Hamzavi, I.H.; Lim, H.W. Photoprotection beyond Ultraviolet Radiation: A Review of Tinted Sunscreens. *J. Am. Acad. Dermatol.* **2021**, *84*, 1393–1397. [[CrossRef](#)]
25. Nazaraly, M.; Wallez, G.; Chanéac, C.; Tronc, E.; Ribot, F.; Quarton, M.; Jolivet, J.P. The First Structure of a Cerium(IV) Phosphate: Ab Initio Rietveld Analysis of $\text{Ce}^{\text{IV}}(\text{PO}_4)(\text{HPO}_4)_{0.5}(\text{H}_2\text{O})_{0.5}$. *Angew. Chem. Int. Ed.* **2005**, *44*, 5691–5694. [[CrossRef](#)]
26. Tong, H.N.; Zhang, H.; Cheng, W.D.; Wu, D.S.; Gong, Y.J.; Zhu, J.; Huang, S.P.; Zhao, D. Synthesis, structure and optical properties of cerium(III) triphosphate CeP_3O_9 . *Chin. J. Struct. Chem.* **2007**, *26*, 338–346.
27. Nazaraly, M.; Wallez, G.; Chanéac, C.; Tronc, E.; Ribot, F.; Quarton, M.; Jolivet, J.P. Synthesis and Characterization of $\text{Ce}^{\text{IV}}(\text{PO}_4)(\text{HPO}_4)_{0.5}(\text{H}_2\text{O})_{0.5}$. *J. Phys. Chem. Solids* **2006**, *67*, 1075–1078. [[CrossRef](#)]
28. Brandel, V.; Clavier, N.; Dacheux, N. Synthesis and Characterization of Uranium(IV) Phosphate-Hydrogenphosphate Hydrate and Cerium(IV) Phosphate-Hydrogenphosphate Hydrate. *J. Solid State Chem.* **2005**, *178*, 1054–1063. [[CrossRef](#)]
29. Clavier, N.; Mesbah, A.; Szenknect, S.; Dacheux, N. Monazite, Rhabdophane, Xenotime & Churchite: Vibrational Spectroscopy of Gadolinium Phosphate Polymorphs. *Spectrochim. Acta Part A Mol. Biomol. Spectrosc.* **2018**, *205*, 85–94. [[CrossRef](#)] [[PubMed](#)]
30. Skogareva, L.S.; Shekunova, T.O.; Baranchikov, A.E.; Yapryntsev, A.D.; Sadovnikov, A.A.; Ryumin, M.A.; Minaeva, N.A.; Ivanov, V.K. Synthesis of Cerium Orthophosphates with Monazite and Rhabdophane Structure from Phosphoric Acid Solutions in the Presence of Hydrogen Peroxide. *Russ. J. Inorg. Chem.* **2016**, *61*, 1219–1224. [[CrossRef](#)]
31. Masui, T.; Hirai, H.; Imanaka, N.; Adachi, G. Characterization and Thermal Behavior of Amorphous Cerium Phosphate. *Phys. Status Solidi* **2003**, *198*, 364–368. [[CrossRef](#)]
32. Garcia-Lodeiro, I.; Irisawa, K.; Jin, F.; Meguro, Y.; Kinoshita, H. Reduction of Water Content in Calcium Aluminate Cement with/out Phosphate Modification for Alternative Cementation Technique. *Cem. Concr. Res.* **2018**, *109*, 243–253. [[CrossRef](#)]
33. Kosacki, I.; Suzuki, T.; Anderson, H.U.; Colomban, P. Raman Scattering and Lattice Defects in Nanocrystalline CeO_2 Thin Films. *Solid State Ion.* **2002**, *149*, 99–105. [[CrossRef](#)]
34. Ivanov, V.K.; Shcherbakov, A.B.; Usatenko, A. V Structure-Sensitive Properties and Biomedical Applications of Nanodispersed Cerium Dioxide. *Russ. Chem. Rev.* **2009**, *78*, 855–871. [[CrossRef](#)]
35. Loridant, S. Raman Spectroscopy as a Powerful Tool to Characterize Ceria-Based Catalysts. *Catal. Today* **2021**, *373*, 98–111. [[CrossRef](#)]
36. Sato, T.; Yin, S. Morphology Control of Cerium Phosphates for Uv-Shielding Application. *Phosphorus Res. Bull.* **2010**, *24*, 43–48. [[CrossRef](#)]
37. Meng, F.; Li, H.; Gong, J.; Fan, Z. Photocatalytic and Magnetic Properties of Loosened Ceria Hollow Microspheres Synthesized by a Single-Step Hydrothermal Method. *J. Mater. Sci. Mater. Electron.* **2016**, *27*, 8433–8439. [[CrossRef](#)]
38. Wang, W.; Zhang, B.; Jiang, S.; Bai, H.; Zhang, S. Use of CeO_2 Nanoparticles to Enhance UV-Shielding of Transparent Regenerated Cellulose Films. *Polymers* **2019**, *11*, 458. [[CrossRef](#)] [[PubMed](#)]
39. Fang, Y.-P.; Xu, A.-W.; Song, R.-Q.; Zhang, H.-X.; You, L.-P.; Yu, J.C.; Liu, H.-Q. Systematic Synthesis and Characterization of Single-Crystal Lanthanide Orthophosphate Nanowires. *J. Am. Chem. Soc.* **2003**, *125*, 16025–16034. [[CrossRef](#)] [[PubMed](#)]
40. Chen, H.; Ni, Y.; Ma, X. Phase-Controllable Synthesis, Shape Evolution and Optical Performances of CePO_4 Nanocrystals via a Simple Oil-Bath Route. *RSC Adv.* **2014**, *4*, 36553. [[CrossRef](#)]
41. Al Mamun, M.A.; Noor, M.; Ullah, A.K.M.A.; Hossain, M.S.; Abdul, M.; Islam, F.; Hakim, M.A. Effect of CePO_4 on Structural, Magnetic and Optical Properties of Ceria Nanoparticles. *Mater. Res. Express* **2018**, *6*, 016102. [[CrossRef](#)]
42. Chen, G.; Baccaro, S.; Nikl, M.; Cecilia, A.; Du, Y.Y.; Mihokova, E. The Red-Shift of Ultraviolet Spectra and the Relation to Optical Basicity of Ce-Doped Alkali Rare-Earth Phosphate Glasses. *J. Am. Ceram. Soc.* **2004**, *87*, 1378–1380. [[CrossRef](#)]
43. Chen, M.Y.; Zu, X.T.; Xiang, X.; Zhang, H.L. Effects of Ion Irradiation and Annealing on Optical and Structural Properties of CeO_2 Films on Sapphire. *Phys. B Condens. Matter* **2007**, *389*, 263–268. [[CrossRef](#)]
44. Elaziouti, A.; Laouedj, N.; Bekka, A.; Vannier, R.-N. Preparation and Characterization of p-n Heterojunction $\text{CuBi}_2\text{O}_4/\text{CeO}_2$ and Its Photocatalytic Activities under UVA Light Irradiation. *J. King Saud Univ. Sci.* **2015**, *27*, 120–135. [[CrossRef](#)]
45. Verma, R.; Samdarshi, S.K.; Bojja, S.; Paul, S.; Choudhury, B. A Novel Thermophotocatalyst of Mixed-Phase Cerium Oxide ($\text{CeO}_2/\text{Ce}_2\text{O}_3$) Homocomposite Nanostructure: Role of Interface and Oxygen Vacancies. *Sol. Energy Mater. Sol. Cells* **2015**, *141*, 414–422. [[CrossRef](#)]
46. Noor, M.; Al Mamun, M.A.; Atique Ullah, A.K.M.; Matsuda, A.; Kawamura, G.; Hakim, M.A.; Islam, M.F.; Matin, M.A. Physics of $\text{Ce}^{3+} \leftrightarrow \text{Ce}^{4+}$ Electronic Transition in Phytosynthesized $\text{CeO}_2/\text{CePO}_4$ Nanocomposites and Its Antibacterial Activities. *J. Phys. Chem. Solids* **2021**, *148*, 109751. [[CrossRef](#)]
47. Kolesnik, I.V.; Shcherbakov, A.B.; Kozlova, T.O.; Kozlov, D.A.; Ivanov, V.K. Comparative Analysis of Sun Protection Characteristics of Nanocrystalline Cerium Dioxide. *Russ. J. Inorg. Chem.* **2020**, *65*, 960–966. [[CrossRef](#)]
48. Rodrigues, N.D.N.; Stavros, V.G. From fundamental science to product: A bottom-up approach to sunscreen development. *Sci. Prog.* **2018**, *101*, 8–31. [[CrossRef](#)]

49. Bouddouch, A.; Amaterz, E.; Bakiz, B.; Taoufyq, A.; Guinneton, F.; Villain, S.; Valmalette, J.C.; Gavarri, J.R.; Benlhachemi, A. Photocatalytic and Photoluminescence Properties of CePO₄ Nanostructures Prepared by Coprecipitation Method and Thermal Treatment. *Optik* **2021**, *238*, 166683. [[CrossRef](#)]
50. Zholobak, N.M.; Ivanov, V.K.; Shcherbakov, A.B.; Shaporev, A.S.; Polezhaeva, O.S.; Baranchikov, A.Y.; Spivak, N.Y.; Tretyakov, Y.D. UV-Shielding Property, Photocatalytic Activity and Photocytotoxicity of Ceria Colloid Solutions. *J. Photochem. Photobiol. B Biol.* **2011**, *102*, 32–38. [[CrossRef](#)]
51. Shekunova, T.O.; Lapkina, L.A.; Shcherbakov, A.B.; Meshkov, I.N.; Ivanov, V.K.; Tsivadze, A.Y.; Gorbunova, Y.G. Deactivation of Singlet Oxygen by Cerium Oxide Nanoparticles. *J. Photochem. Photobiol. A Chem.* **2019**, *382*, 111925. [[CrossRef](#)]
52. Coronado, J.M.; Javier Maira, A.; Martínez-Arias, A.; Conesa, J.C.; Soria, J. EPR Study of the Radicals Formed upon UV Irradiation of Ceria-Based Photocatalysts. *J. Photochem. Photobiol. A Chem.* **2002**, *150*, 213–221. [[CrossRef](#)]
53. Shao, Y.; Ma, Y. Mesoporous CeO₂ Nanowires as Recycled Photocatalysts. *Sci. China Chem.* **2012**, *55*, 1303–1307. [[CrossRef](#)]
54. Wandre, T.M.; Gaikwad, P.N.; Tapase, A.S.; Garadkar, K.M.; Vanalakar, S.A.; Lokhande, P.D.; Sasikala, R.; Hankare, P.P. Sol–Gel Synthesized TiO₂–CeO₂ Nanocomposite: An Efficient Photocatalyst for Degradation of Methyl Orange under Sunlight. *J. Mater. Sci. Mater. Electron.* **2016**, *27*, 825–833. [[CrossRef](#)]
55. Tang, Z.-R.; Zhang, Y.; Xu, Y.-J. A Facile and High-Yield Approach to Synthesize One-Dimensional CeO₂ Nanotubes with Well-Shaped Hollow Interior as a Photocatalyst for Degradation of Toxic Pollutants. *RSC Adv.* **2011**, *1*, 1772. [[CrossRef](#)]
56. Vinothkumar, G.; Lalitha, A.I.; Suresh Babu, K. Cerium Phosphate–Cerium Oxide Heterogeneous Composite Nanozymes with Enhanced Peroxidase-Like Biomimetic Activity for Glucose and Hydrogen Peroxide Sensing. *Inorg. Chem.* **2019**, *58*, 349–358. [[CrossRef](#)] [[PubMed](#)]
57. Zeng, Y.; Wang, Y.; Zhang, S.; Zhong, Q.; Rong, W.; Li, X. One-Pot Synthesis of Ceria and Cerium Phosphate (CeO₂-CePO₄) Nanorod Composites for Selective Catalytic Reduction of NO with NH₃: Active Sites and Reaction Mechanism. *J. Colloid Interface Sci.* **2018**, *524*, 8–15. [[CrossRef](#)] [[PubMed](#)]
58. Fijolek, L.; Wolski, L. Bifunctional CePO₄/CeO₂ Nanocomposite as a Promising Heterogeneous Catalyst for the Enhancement of the Ozonation Recovery Effect in the Presence of Chloride Ions. *Sci. Rep.* **2022**, *12*, 9043. [[CrossRef](#)] [[PubMed](#)]
59. Hirano, S.; Suzuki, K.T. Exposure, Metabolism, and Toxicity of Rare Earths and Related Compounds. *Environ. Health Perspect.* **1996**, *104*, 85–95. [[CrossRef](#)] [[PubMed](#)]
60. Pulido-Reyes, G.; Rodea-Palomares, I.; Das, S.; Sakthivel, T.S.; Leganes, F.; Rosal, R.; Seal, S.; Fernández-Pinãs, F. Untangling the Biological Effects of Cerium Oxide Nanoparticles: The Role of Surface Valence States. *Sci. Rep.* **2015**, *5*, 15613. [[CrossRef](#)]
61. Liu, Y.; Ma, Y.; Jiao, C.; Liu, M.; Luo, W.; Dong, C.; Fan, S.; He, X.; Yang, F.; Zhang, Z. Comparative Toxicity of Rod-Shaped Nano-CeO₂ and Nano-CePO₄ to Lettuce. *Metallomics* **2021**, *13*, mfab033. [[CrossRef](#)]
62. Clavier, N.; Podor, R.; Dacheux, N. Crystal Chemistry of the Monazite Structure. *J. Eur. Ceram. Soc.* **2011**, *31*, 941–976. [[CrossRef](#)]
63. Dacheux, N.; Clavier, N.; Podor, R. Monazite as a Promising Long-Term Radioactive Waste Matrix: Benefits of High-Structural Flexibility and Chemical Durability. *Am. Mineral.* **2013**, *98*, 833–847. [[CrossRef](#)]
64. Achary, S.N.; Bevara, S.; Tyagi, A.K. Recent Progress on Synthesis and Structural Aspects of Rare-Earth Phosphates. *Coord. Chem. Rev.* **2017**, *340*, 266–297. [[CrossRef](#)]
65. Rozhin, P.; Melchionna, M.; Fornasiero, P.; Marchesan, S. Nanostructured Ceria: Biomolecular Templates and (Bio)Applications. *Nanomaterials* **2021**, *11*, 2259. [[CrossRef](#)] [[PubMed](#)]
66. Walther, R.; Huynh, T.H.; Monge, P.; Fruergaard, A.S.; Mamakhel, A.; Zelikin, A.N. Ceria Nanozyme and Phosphate Prodrugs: Drug Synthesis through Enzyme Mimicry. *ACS Appl. Mater. Interfaces* **2021**, *13*, 25685–25693. [[CrossRef](#)]
67. Ni, P.; Wei, X.; Guo, J.; Ye, X.; Yang, S. On the Origin of the Oxidizing Ability of Ceria Nanoparticles. *RSC Adv.* **2015**, *5*, 97512–97519. [[CrossRef](#)]
68. De Marzi, L.; Monaco, A.; De Lapuente, J.; Ramos, D.; Borrás, M.; Di Gioacchino, M.; Santucci, S.; Poma, A. Cytotoxicity and Genotoxicity of Ceria Nanoparticles on Different Cell Lines in Vitro. *Int. J. Mol. Sci.* **2013**, *14*, 3065–3077. [[CrossRef](#)] [[PubMed](#)]

Disclaimer/Publisher’s Note: The statements, opinions and data contained in all publications are solely those of the individual author(s) and contributor(s) and not of MDPI and/or the editor(s). MDPI and/or the editor(s) disclaim responsibility for any injury to people or property resulting from any ideas, methods, instructions or products referred to in the content.